Behavioral/Systems/Cognitive

Cranial Visceral Afferent Pathways through the Nucleus of the Solitary Tract to Caudal Ventrolateral Medulla or Paraventricular Hypothalamus: Target-Specific Synaptic Reliability and Convergence Patterns

Timothy W. Bailey,[1] Sam M. Hermes,[2] Michael C. Andresen,[1] and Sue A. Aicher[2]

[1]Department of Physiology and Pharmacology and [2]Neurological Sciences Institute, Oregon Health & Science University, Portland, Oregon 97239-3098

Cranial visceral afferents activate central pathways that mediate systemic homeostatic processes. Afferent information arrives in the brainstem nucleus of the solitary tract (NTS) and is relayed to other CNS sites for integration into autonomic responses and complex behaviors. Little is known about the organization or nature of processing within NTS. We injected fluorescent retrograde tracers into two nuclei to identify neurons that project to sites involved in autonomic regulation: the caudal ventrolateral medulla (CVLM) or paraventricular nucleus of the hypothalamus (PVN). We found distinct differences in synaptic connections and performance in the afferent path through NTS to these neurons. Anatomical studies using confocal and electron microscopy found prominent, primary afferent synapses directly on somata and dendrites of CVLM-projecting NTS neurons identifying them as second-order neurons. In brainstem slices, afferent activation evoked large, constant latency EPSCs in CVLM-projecting NTS neurons that were consistent with the precise timing and rare failures of monosynaptic contacts on second-order neurons. In contrast, most PVN-projecting NTS neurons lacked direct afferent input and responded to afferent stimuli with highly variable, intermittently failing synaptic responses, indicating polysynaptic pathways to higher-order neurons. The afferent-evoked EPSCs in most PVN-projecting NTS neurons were smaller and unreliable but also often included multiple, convergent polysynaptic responses not observed in CVLM-projecting neurons. A few PVN-projecting NTS neurons had monosynaptic EPSC characteristics. Together, we found that cranial visceral afferent pathways are structured distinctly within NTS depending on the projection target. Such, intra-NTS pathway architecture will substantially impact performance of autonomic or neuroendocrine reflex arcs.

Key words: **paraventricular; brainstem; hypothalamus; autonomic; sensory; baroreceptor**

Introduction

For many homeostatic reflexes, the principal pathway begins with cranial visceral afferents entering the CNS at the nucleus of the solitary tract (NTS). This afferent information is projected to diverse sites, including efferent nuclei within brainstem, spinal cord, and hypothalamus (Pilowsky and Goodchild, 2002; Guyenet, 2006). Although the simplest of these reflexes can consist of as few as two central neurons, a broad complement of CNS nuclei also process afferent signals that are relayed from NTS as part of an orchestrated integration with complex behaviors (Spyer, 1990). Two prominent nuclei that play very different roles in autonomic regulation are contained within the caudal ventrolateral medulla (CVLM) (Jeske et al., 1993; Aicher et al., 1996) and the paraventricular nucleus of the hypothalamus (PVN) (Stern, 2001; Benarroch, 2005). CVLM contains the critical intermediary neurons in the baroreflex pathway that mediate baroreceptor-initiated sympathoinhibition of sympathetic neurons within the rostral ventrolateral medulla (Aicher et al., 1995). PVN receives dense inputs from NTS (Ruggiero et al., 1994) that impact a mix of reflex outcomes from PVN that integrate neuroendocrine, stress, and homeostatic responses (Chen and Toney, 2003; Herman et al., 2003; Dampney et al., 2005; Guyenet, 2006). Neurons in these two regions display qualitatively different responses to baroreceptor afferent activation. CVLM neurons often display activity patterns that closely follow the pressure profile of each cardiac cycle (Jeske et al., 1993; Schreihofer and Guyenet, 2003), and raising blood pressure activates c-Fos in medial NTS neurons that send axons to CVLM (Weston et al., 2003). Such cardiovascular rhythms and baroreceptor responsiveness are only observed in a subpopulation of spinally projecting PVN neurons (Chen and Toney, 2003), whereas activation of arterial baroreceptors evokes few activity changes in most PVN neurons (Kannan and Yamashita, 1983; Duan et al., 1999). Such results are consistent with substantially different afferent processing along

Received May 12, 2006; revised Oct. 8, 2006; accepted Oct. 10, 2006.

This work was supported by National Institutes of Health Grants HL-70433 (T.W.B.), HL-41119 (M.C.A.), HL-83115 (M.C.A.), and HL-56301 (S.A.A.) and Shared Instrumentation Grant RR-016858 (J. P. Welsh). The electron microscopy was made possible by an instrumentation grant from the M. J. Murdock Charitable Trust. We acknowledge the skilled technical assistance of Jennifer Mitchell, Marc Silverman, James F. Castano, and Dr. Deborah Hegarty.

Correspondence should be addressed to Dr. Timothy W. Bailey, Department of Physiology and Pharmacology, Oregon Health & Science University, Portland, OR 97239-3098. E-mail: bailey.ohsu@gmail.com.

DOI:10.1523/JNEUROSCI.2044-06.2006

 0270-6474/06/2611893-10$15.00/0

the pathways reaching neurons within CVLM compared with those in PVN. Because CVLM- and PVN-projecting NTS neurons are distinct populations of neurons (Hermes et al., 2006), we hypothesized that the pathway from cranial visceral afferents through NTS have target-specific characteristics.

Here, we used fluorescent retrograde tracers to identify NTS neurons that project to either CVLM or PVN. Confocal and electron microscopic studies found prominent anterogradely labeled vagal afferent terminals on CVLM-projecting NTS neurons that anatomically identified them as second-order neurons within cranial visceral afferent pathways. In horizontal brainstem slices, activation of afferent axons within the solitary tract (ST) evoked short-latency, low-jitter EPSCs in all CVLM-projecting NTS neurons, functional properties consistent with monosynaptic transmission (Doyle and Andresen, 2001). In contrast, most PVN-projecting NTS neurons lacked prominent anatomical inputs from vagal afferents and displayed variable synaptic responses to ST activation that were weaker and less reliable and that indicate polysynaptic intra-NTS pathways from ST afferents. Together, our findings indicate pronounced differences in the organization and processing of cranial visceral afferent information within NTS that vary according to the projection target. These intra-NTS differences may strongly impact afferent signals directed to individual autonomic or neuroendocrine reflex arcs and affect reflex performance at a very early stage.

Materials and Methods

All animal procedures were conducted with the approval of the Institutional Animal Care and Use Committee in accordance with the United States Public Health Service Policy on Humane Care and Use of Laboratory Animals and the National Institutes of Health *Guide for the Care and Use of Laboratory Animals*. Male Sprague Dawley rats (Charles River Laboratories, Boston, MA; Taconic Farms, Germantown, NY) were used in all experiments.

Retrograde tract tracing identifies specific projection neurons in NTS. Retrograde tracers rely on somewhat different uptake mechanisms, and individual tracers have different physical properties, including diffusivity and differences in procedure that could influence labeling efficiency and detection of neurons. To control for these differences, three different retrograde tracers were used to identify NTS projection neurons: 1,1′-dioctadecyl-3,3,3′,3′-tetramethyindocarbocyanine perchlorate (DiI) (0.5% in ethanol; Invitrogen, Carlsbad, CA), red RetroBeads (rhodamine; LumaFluor, Naples, FL), or FluoroGold (2% in saline; Fluorochrome, Englewood, CO).

CVLM injections. Rats (230–270 g) were anesthetized with isoflurane (4% for induction, 2% for maintenance), and tracers were pressure injected (Picospritzer II; General Valve, Fairfield, NJ) as described previously (Hermes et al., 2006). Stereotaxic coordinates were 1.0 mm rostral, 1.9–2.0 mm lateral, and 1.9–2.0 mm ventral from calamus scriptorius. Tracer volumes were 50–100 nl for FluoroGold and 50–120 nl for rhodamine.

PVN injections. In one group of rats (40–70 g), DiI was injected iontophoretically using positive current (0.1–1 μA; 10 s on/off cycles; 1.5–3 min) as described previously (Bailey et al., 2003; Doyle et al., 2004). Briefly, these small rats were anesthetized with intramuscular injections (1 ml/kg body weight) of a mixture (ketamine, 56 mg/ml; xylazine, 6 mg/ml; and acepromazine, 1 mg/ml) and mounted in a stereotaxic apparatus. To accommodate these small rats, the incisor bar was 5 mm above horizontal, and stereotaxic arms canted 10° lateral from vertical. Left PVN was targeted at coordinates of 0.4 mm rostral, 1.65 mm lateral, and 6.75–6.8 mm ventral to bregma in these DiI rats. In much larger rats (230–270 g) anesthetized with isoflurane, the stereotaxic incisor bar was set 9 mm below horizontal, and the arms were vertical. For these rats, the PVN coordinates were 1.9 mm caudal, 0.6 mm lateral, and 7.6 mm ventral from bregma. Either rhodamine (115–320 nl) or FluoroGold (150–200 nl) was pressure injected into the left PVN as described previously (Hermes et al., 2006).

In all cases, pipettes were left in place for 5 min after the injection to minimize leakage of the tracer along the pipette track. After wound closure and monitored recovery, rats were returned to the colony. Animals survived 6 to 9 d after rhodamine and FluoroGold injections and up to 12 weeks after DiI injections. Proper targeting of CVLM or PVN was confirmed *post hoc* by direct examination of the injection site. Inadvertent injections outside the targeted region were excluded from study, but injection sites in the forebrain that did not involve PVN yielded no retrogradely labeled neurons in NTS (data not shown) (Hermes et al., 2006). Distributions of labeled cell bodies within NTS for different dyes injected into each target were similar so that all results were combined for reporting.

Combined anterograde labeling of cranial afferents and retrograde labeling of NTS projection neurons. To anatomically examine cranial visceral afferent input to NTS projection neurons, an anterograde tracer was used to label vagal afferents and a retrograde tracer labeled a population of NTS projection neurons. In each rat (180–350 g), the retrograde tracer FluoroGold was injected into either CVLM or PVN, followed by an injection of the anterograde tracer biotinylated dextran amine (BDA) [5–7 μl; 10% in 0.1 M phosphate buffer (PB); Invitrogen] into the ipsilateral nodose ganglion as described previously (Aicher et al., 1999). After the injections, surgical wounds were sutured, and the animal was monitored during recovery from anesthesia and then returned to the animal colony.

Perfusion and immunocytochemistry. Six to 8 d after tracer injections, animals were overdosed with sodium pentobarbital (150 mg/kg, i.p.) and perfused transcardially through the ascending aorta with 200 ml of heparinized saline (1000 U/ml), followed by 50 ml of 3.8% acrolein in 2% paraformaldehyde, pH 7.4, and 200 ml of 2% paraformaldehyde in 0.1 M PB, pH 7.4. Coronal sections (40 μm for NTS, 50 μm for injection sites) were prepared using a vibrating microtome. Alternate sections of NTS from each case were processed for confocal and electron microscopy.

For confocal microscopy, FluoroGold was detected immunocytochemically (rabbit anti-FluoroGold, 1:15,000; Chemicon, Temecula, CA) as described previously (Aicher et al., 1995, 1997, 1999) and was visualized using a secondary antibody conjugated to Alexa 488 (1:800; Invitrogen). BDA was visualized with streptavidin conjugated to Alexa 546 (6.25 μg/ml; Invitrogen) in 0.1 M Tris-saline, pH 7.6, for 2 h at room temperature. Sections were sequentially rinsed in Tris-saline, 0.1 M PB, and 0.05 M PB and then mounted onto gelatin-coated slides. Sections were air dried and coverslipped with Prolong Antifade Media (Invitrogen). For electron microscopic detection of FluoroGold and BDA labeling, BDA was visualized using an avidin–biotin peroxidase detection method, and FluoroGold was detected using an immunogold method (Aicher et al., 1995, 1997, 1999).

Afferent contacts on retrogradely labeled NTS neurons. To visualize the overall pattern of potential afferent contacts to CVLM- and PVN-projecting neurons, we used confocal microscopy of the complementary fluorophores. Confocal analyses of anterogradely labeled vagal afferent contacts onto retrogradely labeled NTS projection neurons were evaluated in cases with successful labeling. Cases were deemed successful with respect to FluoroGold if injection sites into CVLM and PVN were appropriately located, and retrogradely labeled neurons were found within NTS (Hermes et al., 2006). Successful anterograde labeling with BDA occurred when an abundance of labeled axons were seen within NTS (see Fig. 1). Images of the relationship between FluoroGold-labeled neurons and BDA-labeled vagal afferents were captured at 63× from 40 μm sections containing medial NTS from each animal using the single-pass, multi-track format on the Zeiss (Thornwood, NY) LSM 510 scanning confocal microscope. Scans were captured in medial NTS, ipsilateral to injections, between the ST and area postrema, primarily within the dorsomedial subnucleus of NTS. Direct appositions were identified between BDA-labeled varicosities (defined as a profile twice the diameter of the axon of origin) and FluoroGold-labeled cell bodies.

To confirm that appositions seen between BDA-labeled vagal afferents and CVLM-projecting neurons were indeed synaptic, electron microscopic analyses were conducted on CVLM-projecting neurons. Ultrastructural analyses were not conducted on PVN-projecting neurons be-

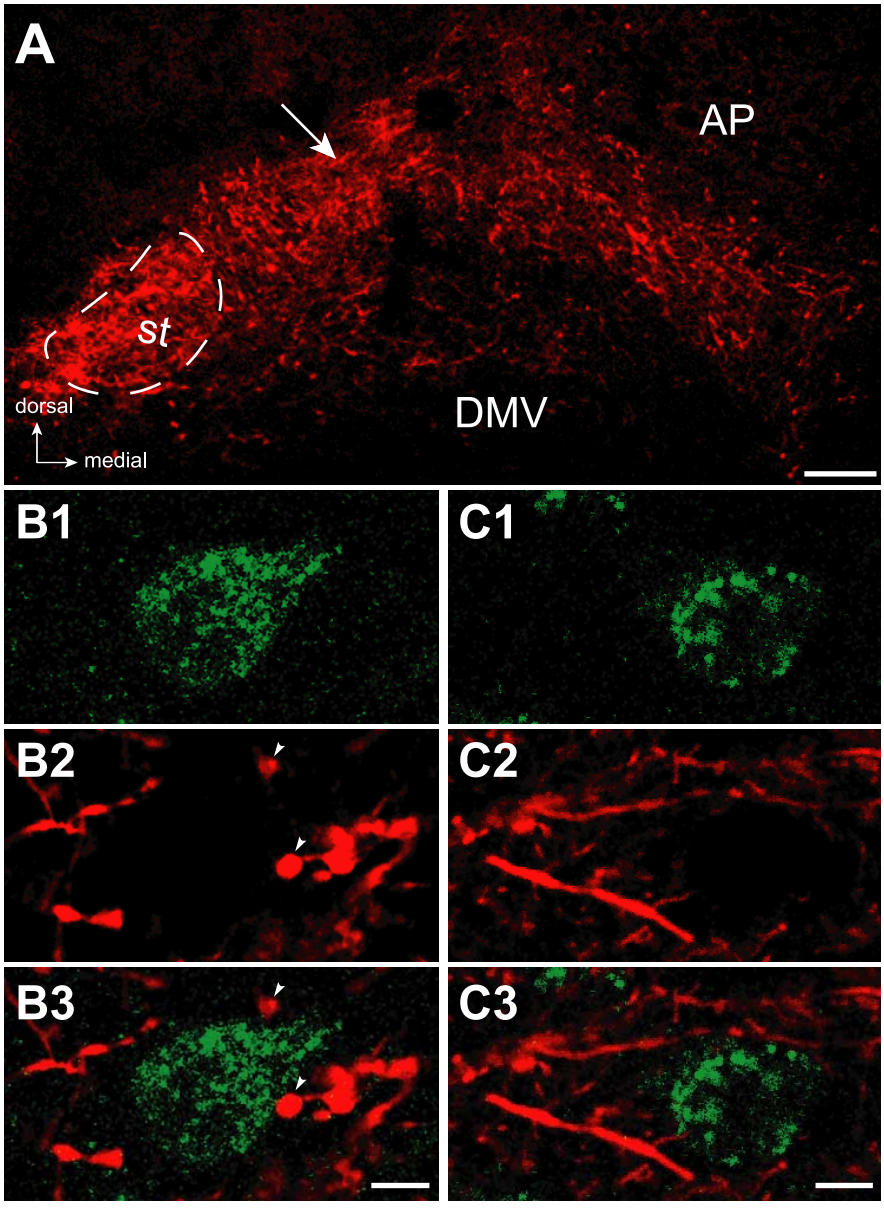

Figure 1. Confocal micrographs show close appositions between anterogradely labeled vagal afferents and retrogradely labeled projection neurons within medial NTS. ***A***, An epifluorescent micrograph shows BDA labeling (red) in medial NTS after injection into the nodose ganglion. Labeling was most intense in dorsomedial NTS (arrow) between the area postrema (AP) and the solitary tract (st; dashed line) but was rarely seen in the dorsal motor nucleus of the vagus (DMV). Dorsal and medial orientations are indicated by arrows (bottom left). ***B***, ***C***, High-magnification confocal micrographs illustrate vagal afferents (red) and retrogradely labeled projection neurons (green) to CVLM (***B***) and PVN (***C***). ***B1***, A single FluoroGold-labeled CVLM-projecting NTS neuron. ***B2***, BDA-labeled vagal afferents within the same optical plane. ***B3***, Overlay shows appositions (arrowheads) between varicosities in vagal afferents and the CVLM-projecting neuron. ***C1***, A single FluoroGold-labeled PVN-projecting NTS neuron. ***C2***, BDA-labeled vagal afferents from the same optical section. ***C3***, Overlay shows vagal axons bypassing the PVN-projecting neuron with no varicosities or appositions. Scale bars: ***A***, 100 μm; ***B***, ***C***, 5 μm.

cause of the paucity of close appositions at the confocal level. For electron microscopic detection of FluoroGold and BDA labeling, BDA was visualized using an avidin–biotin detection method, and FluoroGold was visualized using immunogold detection as described previously (Aicher et al., 1995, 1997, 1999). Ultrathin sections (75 nm) from NTS regions containing both labels were collected onto copper grids, counterstained with uranyl acetate and Reynolds lead citrate, and examined using a Tecnai 12 electron microscope (FEI, Hillsboro, OR). The ultrastructural analysis was conducted on plastic-embedded sections from four animals with optimal preservation of morphological details and maximal detection of labeling. Neurons containing immunogold labeling for FluoroGold were located and evaluated for interactions with axon terminals containing BDA. Regions of tissue containing both labels in close proximity (<1 μm) were captured using a digital camera (2600 × 2600 pixels; Advanced Microscopy Techniques, Danvers, MA).

NTS slices for electrophysiology. On the day of the electrophysiological experiments, rats (200–500 g final weight) with previous retrograde tracer injection were deeply anesthetized with isoflurane. The hindbrain was removed and placed for 1 min in cold (0–2°C) artificial CSF (ACSF) composed of the following (in mM): 125 NaCl, 3 KCl, 1.2 KH_2PO_4, 1.2 $MgSO_4$, 25 $NaHCO_3$, 10 dextrose, and 2 $CaCl_2$ [bubbled with 95%O_2/5%CO_2 as described previously (Doyle and Andresen, 2001)]. The medulla was trimmed to a 1 cm block (rostrocaudal) centered on the caudal end of the fourth ventricle. A wedge of tissue was removed from the ventral surface to align the left ST with the cutting plane when mounted in the vibratome (VT-1000S; Leica, Bannockburn, IL). Slices (250 μm) cut with a sapphire knife (Delaware Diamond Knives, Wilmington, DE) contained the left ST in the same plane as the left NTS. Slices were submerged in a perfusion chamber, and all recordings were performed at 32–36°C and pH 7.4 in ACSF.

Identification and whole-cell recording from labeled NTS neurons. Fluorescence images of cells used in patch-clamp studies were captured under high power on an upright microscope (40×, Axioskop FS2+; Zeiss) equipped with a CCD camera (Zeiss Axiocam HR) controlled by Openlab 3.04 imaging software (Improvision, Lexington, MA). Tracer images were overlaid with rapidly refreshed images made from infrared illumination and differential interference contrast optics (IRDIC). Patch electrodes, 1.8–3.5 MΩ, were guided under IRDIC to cell bodies containing retrograde tracer. Electrodes were filled with a solution composed of the following (in mM): 10 NaCl, 110 K-gluconate, 20 KOH, 11 EGTA, 1 $CaCl_2$, 2 $MgCl_2$, 10 HEPES, 1 NaATP, and 0.1 NaGTP, pH 7.3 (295 mOsm). Whole-cell voltage-clamp recordings were made with Axoclamp 2A or 700B amplifiers (Molecular Devices, Palo Alto, CA). Data were sampled at 50–100 kHz and filtered at 5 kHz via a Molecular Devices 1200 or 1325 analog-to-digital converter and pClamp8 software (Molecular Devices). A concentric bipolar stimulating electrode (200 μm outer diameter; Frederick Haer Company, Bowdoinham, ME) was placed on the ST 1–5 mm from the recording site. Electrical ST stimuli (10–100 μA; two to five times threshold) were delivered from an isolated programmable stimulator (Master-8; A.M.P.I., Jerusalem, Israel) using bursts of five stimuli at 50 Hz repeated every 3–6 s. Latency of ST-evoked EPSCs was calculated as the time from stimulus artifact to the onset of the first EPSC in each train using a differentiated trace (Doyle and Andresen, 2001). Synaptic jitter in each neuron was calculated as the SD of latency to repeated ST shocks ($n > 20$). Synaptic failures were counted as any ST shock that failed to evoke an EPSC. Averages of EPSC amplitude excluded any failed synaptic events. The peak amplitudes of each EPSC in response to bursts of five stimuli of at 50 Hz (EPSC1 to EPSC5) were used to assess frequency-dependent depression (FDD) in each neuron. As

with unlabeled neurons in naive slices, a small percentage of dye-filled neurons did not respond to ST stimulation. Such neurons were excluded from additional study (PVN, $n = 4$; CVLM, $n = 9$) because they may represent neurons with ST connections damaged by slice preparation.

Drugs. 1,2,3,4-Tetrahydro-6-nitro-2, 3-dioxobenzo quinoxaline-7-sulfonamide (NBQX) was obtained from Sigma–RBI (Natick, MA). Capsaicin was obtained from Tocris Cookson (Ballwin, MO).

Statistical analyses. All data are presented as averages ± SEM. Statistical comparisons were made using unpaired Student's *t* test, repeated-measures ANOVA, or one-way ANOVA followed by Fisher's PLSD *post hoc* analysis when appropriate (see individual results; Statview 4.57; Abacus Concepts, Calabasas, CA). *P* values <0.05 indicated significant differences. Except when noted, all tests included an initial ANOVA followed by *post hoc* differences testing, and *p* values cited reflect the results of the final *post hoc* test.

Results

Cranial visceral afferents contact NTS neurons projecting to CVLM or PVN

In animals with both anterogradely labeled vagal afferents and retrogradely labeled projection neurons, we evaluated the relationship between vagal afferent varicosities and CVLM- or PVN-projecting neurons in medial NTS. This region of the NTS receives dense innervation from vagal afferents, including arterial baroreceptors (Ciriello, 1983; Mendelowitz et al., 1992), and also contains neurons that project to either CVLM or PVN (Weston et al., 2003; Hermes et al., 2006). Vagal afferent labeling was intense within ST, and varicose fibers were found in most subnuclei of NTS (Fig. 1*A*). By confocal microscopy, BDA-labeled vagal afferents formed varicosities that often closely apposed the cell bodies of CVLM-projecting NTS neurons (Fig. 1*B*). The presence of axosomatic contacts with NTS neurons is consistent with previous descriptions of various cranial visceral afferents (Miller et al., 1983; Kalia and Richter, 1985; Anders et al., 1993; Maley, 1996; Sekizawa et al., 2003; Doyle et al., 2004). In contrast, many PVN-projecting neurons lacked evidence of axosomatic appositions from varicose vagal afferents (Fig. 1*C*).

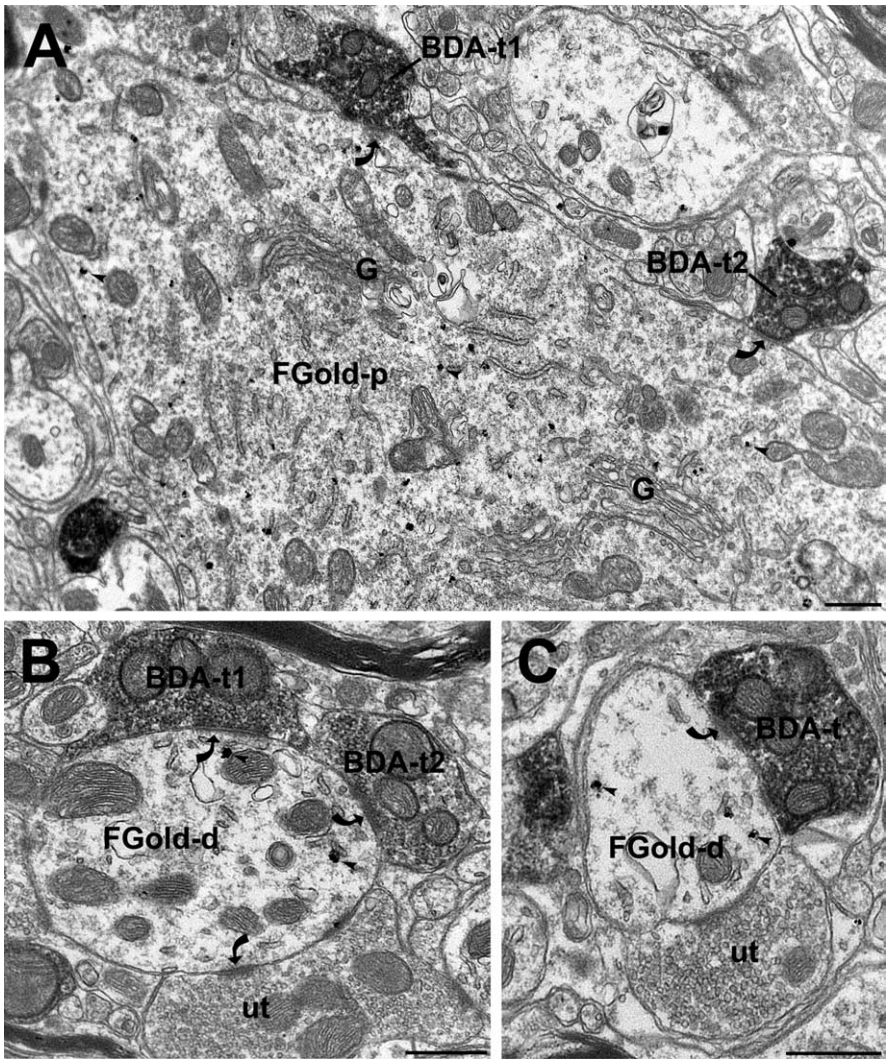

Figure 2. Electron micrographs show BDA-labeled terminals contacting the somata and dendrites of FluoroGold-labeled CVLM-projecting neurons. ***A***, Two BDA-labeled axon terminals (BDA-t1, BDA-t2) form asymmetric synapses (curved arrows) with a FluoroGold-labeled somata (FGold-p). Immunogold labeling for FluoroGold (arrowheads) was found throughout the cytoplasm. G, Golgi apparatus. ***B***, A FluoroGold-labeled dendrite (FGold-d) received asymmetric synapses (curved arrows) from two BDA-labeled axon terminals (BDA-t1, BDA-t2), as well as from an unlabeled axon terminal (ut). ***C***, A FluoroGold-labeled dendrite (FGold-d) received an asymmetric synapse (curved arrow) from a BDA-labeled axon terminal (BDA-t) and received an apposition from an unlabeled axon terminal (ut). Axosomatic contacts were found on 10 different neurons, in addition to 22 axodendritic contacts. Scale bars, 500 nm.

To confirm that the varicose appositions viewed in confocal images of CVLM-projecting NTS neurons were indeed ultrastructurally defined synapses, these cases were examined by electron microscopy. Electron micrographs show the presence of asymmetric synapses between BDA-labeled axon terminals and FluoroGold-labeled neurons (Fig. 2). Vagal afferents formed synapses with both somata (Fig. 2*A*) and dendrites (Fig. 2*B*,*C*) of CVLM-projecting NTS neurons. Consistent with a high density of vagal afferent contacts, multiple BDA-positive synaptic profiles were often encountered in single ultrathin sections even through the soma (Fig. 2*A*). Our studies demonstrate that vagal afferents form direct synaptic contacts with CVLM-projecting NTS neurons, and thus such neurons were anatomically identified as monosynaptically coupled to cranial visceral afferents. Our observations of large visceral afferent synaptic currents (see below) coupled with previous reports of afferent synaptic terminals on NTS neuron somata (Miller et al., 1983; Kalia and Richter, 1985; Anders et al., 1993; Maley, 1996; Sekizawa et al., 2003; Doyle et al., 2004) suggest that proximal cranial visceral afferent contacts are common and contrast the pattern of integration by weak excitatory contacts on distal dendrites so common in other brain regions (Bruno and Sakmann, 2006).

Identification of CVLM- and PVN-projecting neurons in NTS slice

Projection neurons identified with fluorescent retrograde tracers were readily visualized for recording in horizontal NTS slices (Fig. 3*A*,*B*). Brainstems sliced horizontally for electrophysiolog-

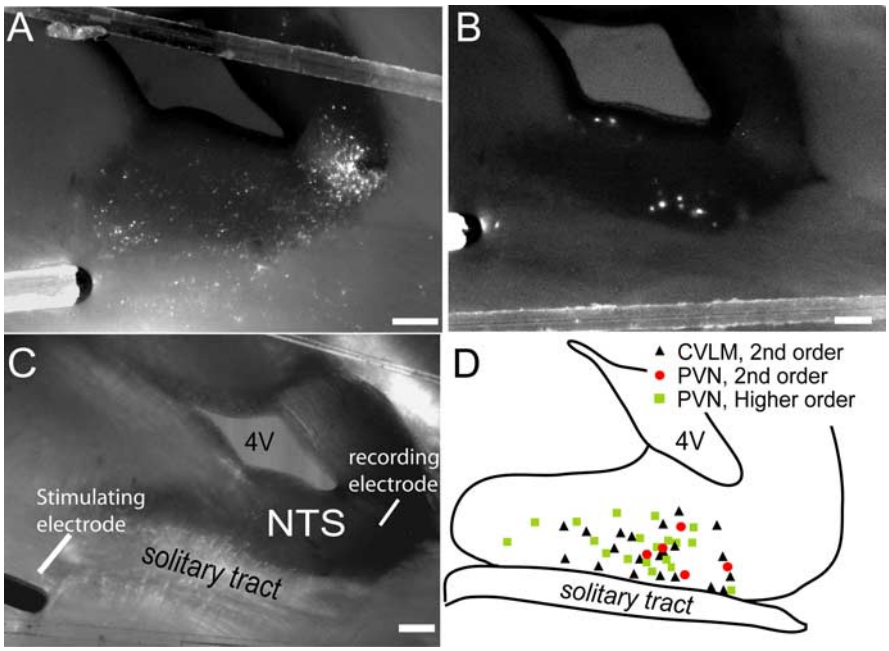

Figure 3. Fluorescent retrograde label injected into either CVLM or PVN marked NTS projection neurons in nearly horizontal slices of brainstem. Low-power fluorescence images of representative horizontal NTS slices with previous tracer injection into CVLM (***A***; rhodamine) or PVN (***B***; DiI). Labeled neurons were distributed throughout the medial NTS. CVLM injections generally labeled more NTS neurons than did PVN injections. ***C***, IRDIC low-power image of a typical horizontal NTS slice preparation showing typical landmarks such as solitary tract and fourth ventricle (4V). Stimulating electrode on ST and typical recording electrode placement are also shown. ***D***, Line drawing shows the relative location of recorded NTS neurons: monosynaptic CVLM-projecting (black triangles; $n = 22$), monosynaptic PVN-projecting (red circles; $n = 5$), and polysynaptic PVN-projecting (green squares; $n = 19$). Scale bars, 200 μm.

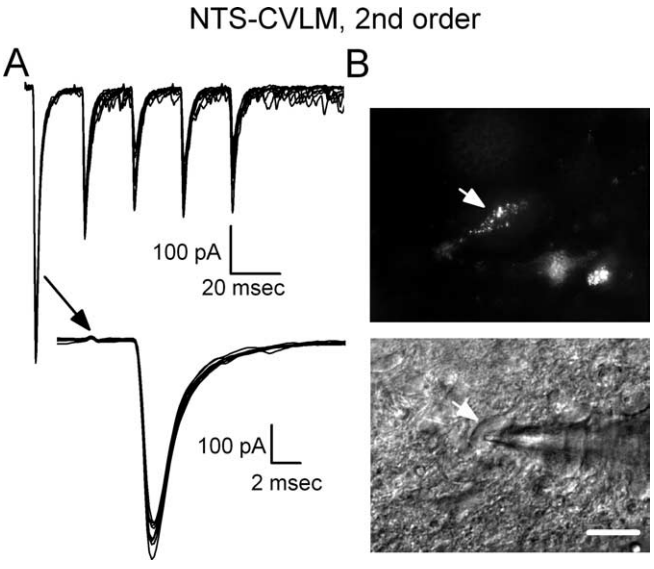

Figure 4. CVLM-projecting NTS neurons exhibit large invariant ST synaptic responses consistent with direct monosynaptic connections from cranial visceral afferents. ***A***, Overlaid traces of ST-evoked EPSCs (for clarity, limited to 10 traces) in a representative CVLM-projecting NTS neuron. ST-evoked EPSCs had very few failures and consistent latency (3.2 ms). The low variability in EPSC latency (45 μs jitter) is clearly evident for the first EPSC in the expanded timescale below. ***B***, Top shows neuron in ***A*** under fluorescence illumination (arrow). Note the accumulation of retrograde tracer (rhodamine beads) throughout the cell body and proximal process. Scale bar, 10 μm. Bottom shows IRDIC image of the same neuron with recording pipette (arrow).

ical studies preserved the ST as a visible stripe coursing rostral to caudal. In addition to the ST, the translucent outline of the NTS and the borders of the fourth ventricle provided anatomical landmarks to identify subregions of NTS (Fig. 3*C*). Medial NTS is bounded by the midline and the ST and extends ~1 mm caudal to the fourth ventricle. All recorded PVN- and CVLM-projecting NTS neurons were scattered within this region (Fig. 3*D*), and the general distribution of CVLM- and PVN-projecting NTS neurons was similar to that observed in fixed tissue preparations of medial NTS (Hermes et al., 2006). There was no apparent topographic separation of projection neurons based on target or electrophysiological criteria (see below) (Fig. 3*D*).

Monosynaptic ST-afferent pathways to CVLM-projecting NTS neurons

In CVLM-projecting NTS neurons ($n = 22$ in 14 slices), ST shocks activated large EPSCs (Fig. 4). ST-EPSCs (Fig. 4) had remarkably consistent waveforms and invariant latencies (jitter <200 μs). Bursts of five ST shocks evoked EPSCs (EPSC1–EPSC5) that progressively depressed in amplitude within each burst, indicating substantial FDD. ST shocks rarely (<1%) failed to elicit an EPSC in CVLM-projecting NTS neurons. Incrementing the stimulus intensity recruited these synaptic responses in an all-or-none manner that is consistent with activation of a single afferent axon (Bailey et al., 2006). Consistent with previous studies (Doyle and Andresen, 2001), NBQX completely blocked ST-EPSCs in these CVLM-projecting cells ($n = 6$). Overall, the characteristics of ST-EPSCs were typical of second-order neurons in medial NTS and indicate a high-release probability, glutamatergic synapse (Doyle and Andresen, 2001; Doyle et al., 2002; Bailey et al., 2006). Thus, the results suggest that CVLM-projecting NTS neurons are coupled to ST afferent inputs via direct, monosynaptic synapses.

Polysynaptic ST-afferent pathways to PVN-projecting NTS neurons

ST shocks activated EPSCs in all ST-coupled PVN-projecting NTS neurons ($n = 24$ in 16 slices). The pattern of ST-evoked EPSCs, however, varied widely both within and across individual neurons (Figs. 5, 6). Most commonly in PVN-projecting neurons, ST shocks evoked EPSCs with quite variable latencies on repeated activation (e.g., jitter, 707 μs in Fig. 5). ST shocks often failed to elicit any response at all in these neurons (Fig. 5*A*, Failures). In addition, the shape and amplitude of ST-EPSCs varied substantially within individual neurons. High synaptic jitter and frequent synaptic failures are consistent with a polysynaptic pathway of transmission from ST afferents to PVN-projecting NTS neurons and imply the presence of intervening interneurons (compare Figs. 4, 5). Interestingly, a minority of PVN-projecting NTS neurons (5 of 24) had ST-evoked EPSC characteristics that closely resembled ST-evoked responses of CVLM-projecting neurons (Fig. 6). Thus, synaptic properties of most PVN-projecting NTS neurons were consistent with an indirect, polyneuronal pathway from ST, but some neurons had synaptic re-

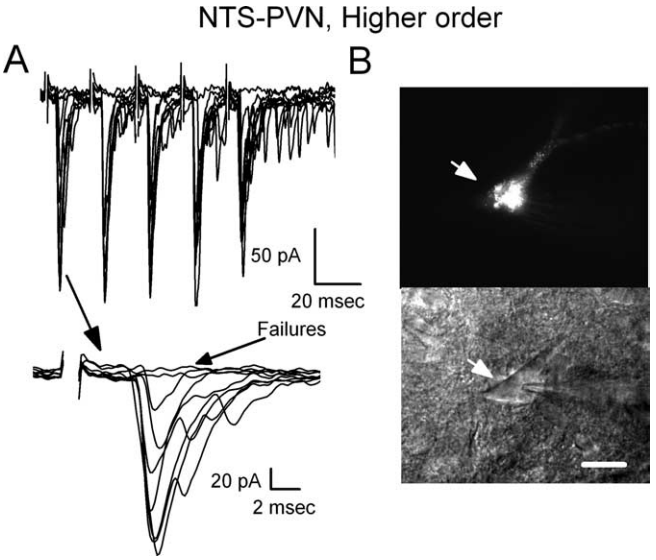

Figure 5. PVN-projecting NTS neurons exhibit highly variable synaptic responses to ST consistent with afferent transmission from cranial visceral afferents through polysynaptic pathways. ***A***, Overlaid traces of ST-evoked EPSCs (for clarity, limited to 10 traces) in a representative PVN-projecting NTS neuron. PVN-projecting neurons exhibited ST-evoked EPSCs that were very inconsistent in latency and amplitude. In this neuron, many ST shocks produced no EPSC, i.e., synaptic failures indicated by flat ST-synched trace. The mean latency was 5.2 ms but initiation of the EPSC was highly variable, as highlighted in the expanded timescale (bottom) of the first EPSC traces (707 μs jitter). These ST-evoked EPSC characteristics are consistent with an indirect path from ST afferents through polysynaptic excitatory connections. ***B***, Top shows a fluorescence image of a recorded neuron (arrow) showing the accumulation of retrograde tracer (rhodamine beads) throughout the cell body and proximal processes. The bottom shows the same cell under IRDIC with recording pipette (arrow). Scale bar, 10 μm.

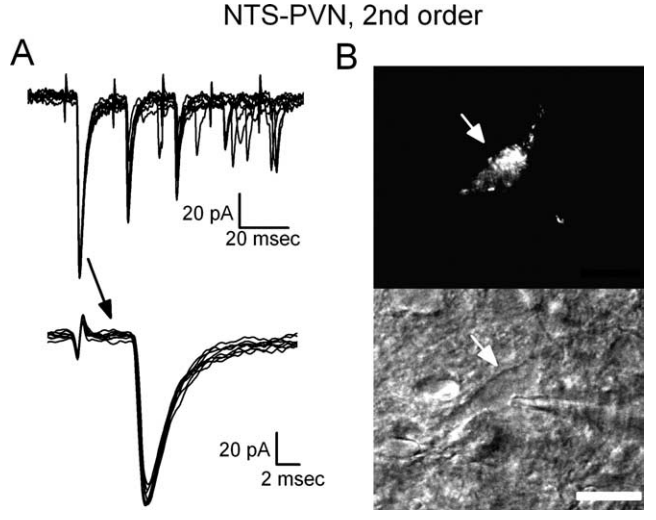

Figure 6. Some PVN-projecting NTS neurons display low-jitter ST-EPSC responses indicating direct, monosynaptic connections from cranial visceral afferents. ***A***, Overlaid current traces of ST-evoked EPSCs (for clarity, limited to 10 traces) in a representative PVN-projecting NTS neuron strongly resemble those typical in NTS neurons projecting to CVLM (see Fig. 4). Latencies of ST-evoked EPSCs had low jitter, consistent with a direct path from ST. ***B***, Top is a fluorescence image of the neuron recorded in ***A*** showing the accumulation of retrograde tracer (rhodamine beads) throughout the cell body and proximal processes. Bottom shows the same neuron under IRDIC with recording pipette (arrow). Scale bar, 10 μm.

sponses consistent with direct contact with ST synapses. All synaptic responses activated in PVN-projecting neurons by ST stimulation were abolished by NBQX (data not shown), whether higher order ($n = 8$) or second order ($n = 4$).

EPSC jitter discriminates CVLM- from PVN-projecting neurons

Comparing across the groups of labeled projection neurons, the ST synaptic transmission characteristics were remarkably uniform across individual neurons for the cohort of CVLM-projecting NTS neurons within medial NTS compared with the widely varying properties of afferent transmission to PVN-projecting neurons. Within individual CVLM-projecting NTS neurons, the ST-EPSC1 latency varied over only a few tens of microseconds, resulting in sharply narrow latency distributions (Fig. 7*A*), but similar histograms for PVN-projecting neurons commonly spanned several milliseconds (Fig. 7*B*). Inspection of response to multiple successive ST shocks revealed frequent synaptic failures only in PVN-projecting neurons (Fig. 7*B*). Quantitatively across all labeled neurons (Fig. 7*C*), the absolute EPSC latency poorly distinguished CVLM- from PVN-projecting neurons because the two populations spanned nearly identical ranges of latency values: approximately from 1 to 10 ms within each group. However, no CVLM-projecting neurons (Fig. 7*C*, black triangles) had an ST-EPSC synaptic jitter >158 μs, despite EPSC latencies as great as 9 ms. In higher-order PVN-projecting NTS neurons (Fig. 7*C*, green squares), the EPSC latency was never <4 ms, approximately double the EPSC latency arriving at second-order, CVLM-projecting neurons. This relatively high EPSC latency value is consistent with participation of an intervening NTS interneuron. Conversely, note that EPSC latency and jitter values for five PVN-projecting neurons (Fig. 7*C*, red circles) were similar to the values for CVLM-projecting neurons, and such PVN-projecting neurons were considered second order (Fig. 6).

Low-amplitude EPSCs and high failure rates characterize the ST–NTS–PVN pathway

ST afferents form uncommonly uniform, unusually high release glutamatergic synapses onto second-order NTS neurons (Bailey et al., 2006). Such high release synapses are prone to strong synaptic depression at high rates of activation (Trussell, 1999; Zucker and Regehr, 2002). In CVLM-projecting NTS neurons, bursts of five closely timed ST shocks (50 Hz) evoked ST-EPSCs with successively smaller amplitudes (Fig. 8*A*,*B*) that reached an average FDD of >50%. High FDD is common in NTS neurons directly coupled to the ST (Doyle and Andresen, 2001). In contrast to higher-order PVN-projecting NTS neurons, identical bursts of ST shocks evoked significantly smaller EPSC1s than those found in CVLM-projecting or PVN-projecting second-order neurons ($p < 0.04$) (Fig. 8*A*). Higher-order PVN-projecting NTS neurons did not display FDD, i.e., successive EPSC1 to EPSC5 amplitudes were equivalent within the 50 Hz burst of ST stimulation ($p > 0.05$) (Fig. 8*B*). Interestingly, low-jitter, second-order PVN-projecting NTS neurons had FDD characteristics that were quantitatively similar to CVLM-projecting NTS neurons (Fig. 8*A*,*B*). Last, the rates of synaptic failure in higher-order PVN-projecting neurons were substantially higher (16.5 ± 3.8% for EPSC1) than for second-order neurons whether CVLM-projecting or PVN-projecting (0.5 ± 0.2 and 0.3 ± 0.3% respectively; $p < 0.003$ for EPSC1). Interestingly, the mean failure rates for higher-order, PVN-projecting neurons were uniformly high for all EPSCs within the burst of stimuli (Fig. 8*C*, EPSC1–EPSC5).

Multiple ST paths converge onto higher-order, PVN-projecting NTS neurons

Despite receiving smaller-amplitude EPSCs, ST stimulation often activated multiple, distinct ST-synchronized inputs to higher-order, PVN-projecting NTS neurons (Fig. 9). In all cases, analysis

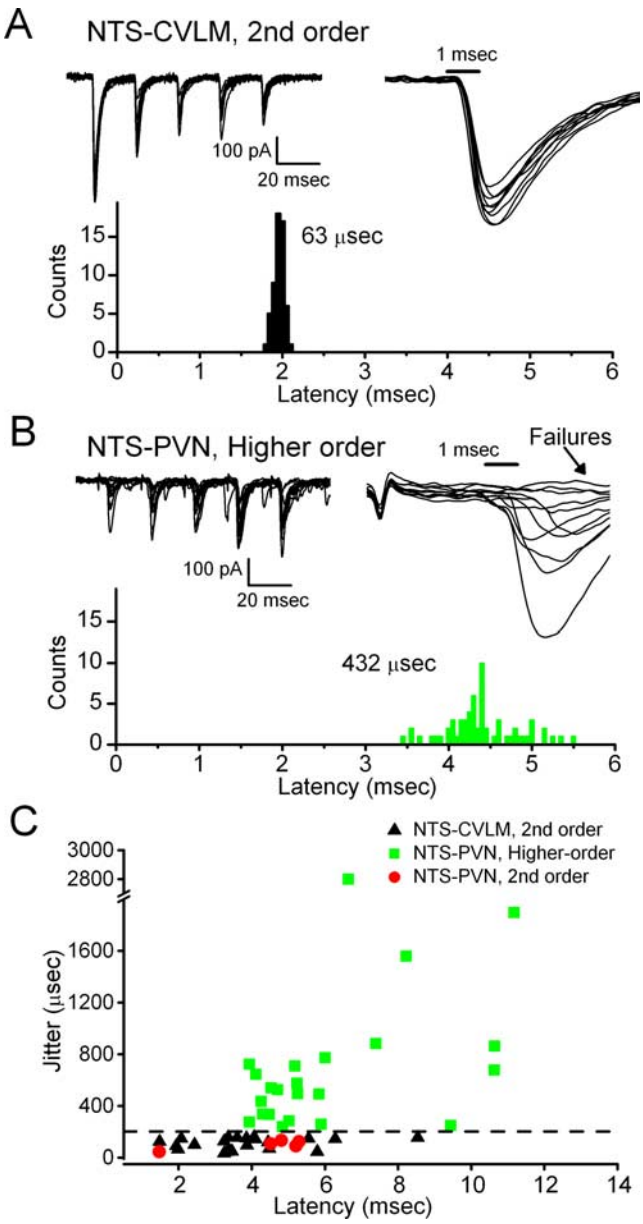

Figure 7. CVLM-projecting NTS neurons were monosynaptically coupled to ST, whereas PVN-projecting neurons were primarily coupled through polysynaptic pathways via NTS interneurons. ***A***, In a representative CVLM-projecting NTS neuron, ST stimuli always evoked an EPSC (top left). The EPSC latency was highly consistent, as highlighted in traces in which the first EPSC in the burst is shown on an expanded timescale (top right). A histogram of EPSC latencies shows a narrow distribution of values, with a total range of <500 μs and a calculated jitter of 63 μs. ***B***, In a representative higher-order PVN-projecting NTS neuron (top left), ST shocks evoked EPSCs at highly variable latencies and variable amplitudes, and note that a large proportion of ST shocks failed to evoke synaptic events (top right). The latency histogram for this neuron showed a very broad distribution of response latencies that covered a range of over 2000 μs with a jitter of 432 μs. ***C***, The summary relationship between jitter and latency for CVLM-projecting (black triangles) and those for second-order (red circles) and higher-order (green squares) PVN-projecting NTS neurons shows that, although absolute latency ranges were fairly similar, high jitters were found only in the PVN-projecting neurons. All CVLM-projecting neurons plus five PVN-projecting neurons had the low jitter values (<200 μs, below dashed line) that were consistent with direct, monosynaptic ST input. Most PVN-projecting neurons had very high jitters and were thus coupled through complex polysynaptic pathways to afferent inputs.

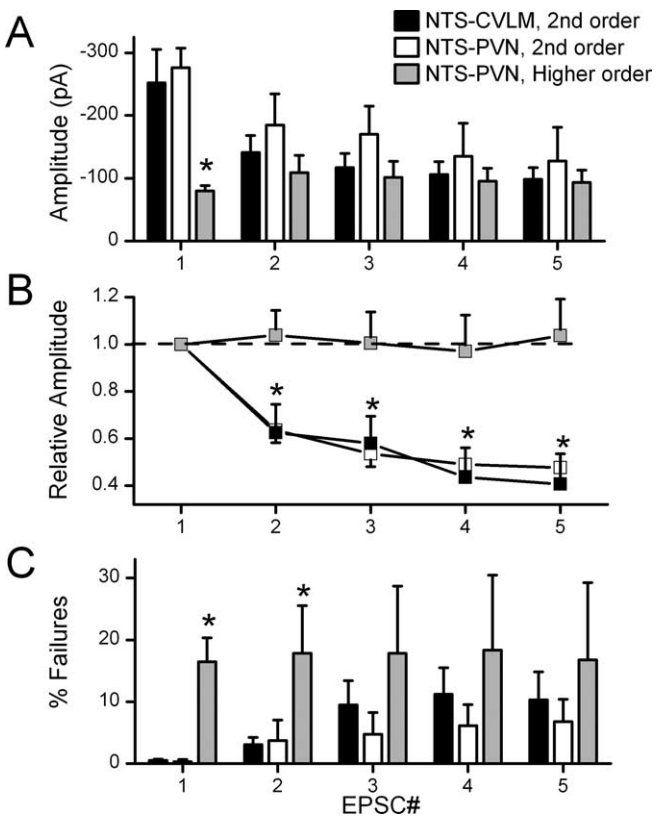

Figure 8. Summary of the EPSC amplitude changes to the burst of five ST stimuli clearly distinguished second from higher-order NTS neurons, whether projecting to CVLM or to PVN. ***A***, Second-order CVLM-projecting ($n = 22$) and PVN-projecting ($n = 5$) NTS neurons expressed similar amplitudes throughout the ST burst from EPSC1 to EPSC5. Higher-order PVN-projecting NTS neurons ($n = 19$) had significantly smaller EPSC1 amplitudes compared with CVLM-projecting and second-order PVN-projecting neurons ($p < 0.035$). ***B***, FDD comparisons between higher-order and second-order neurons are even clearer in plots of these relationships normalized to the EPSC1 amplitude. Higher-order PVN-projecting NTS neurons showed no FDD. This minimal change in EPSC amplitude within burst is different than the robust FDD changes in second-order CVLM-projecting and second-order PVN-projecting neurons ($p < 0.01$). ***C***, Failure rates were quite low in second-order PVN and CVLM-projecting neurons and significantly greater in the higher-order PVN-projecting NTS neuron group at first and second positions within the burst of five shocks ($p < 0.018$). All statistical comparisons are *post hoc* comparisons (Fisher's PLSD test) after repeated measures or one-way ANOVA when appropriate.

of the timing of individual ST-synchronized inputs identified them as arising from indirect, polysynaptic pathways from ST (Fig. 9*A*). Such analysis revealed that each input had unique latency/jitter characteristics as well as independent incidents of failure (Fig. 9*A*). Distributions of event latencies within individual neurons segregated into wide and nonoverlapping event clusters (Fig. 9*A*). The behavior of these convergent intra-NTS inputs resembled the performance of single polysynaptic inputs to higher-order, PVN-projecting neurons. Generally, failure rates across all second-order neurons were quite low (Fig. 9*B*, shaded inset), but higher failure rates in higher-order neurons ranged upward to approach two-thirds of events (Fig. 9*B*), a finding consistent with poor likelihood for successful transmission through intervening interneurons. Note that such high-jitter, ST-synched polysynaptic inputs were never observed in second-order NTS neurons projecting to either CVLM or PVN. The finding of convergent inputs to higher-order PVN neurons activated by single shocks suggest that these ST stimuli must simultaneously activate multiple, different intra-NTS pathways. Such contrasting results in higher-order NTS neurons strengthen the impression that second-order NTS neurons predominantly receive only single ST inputs despite stimuli that activate multiple ST afferent pathways.

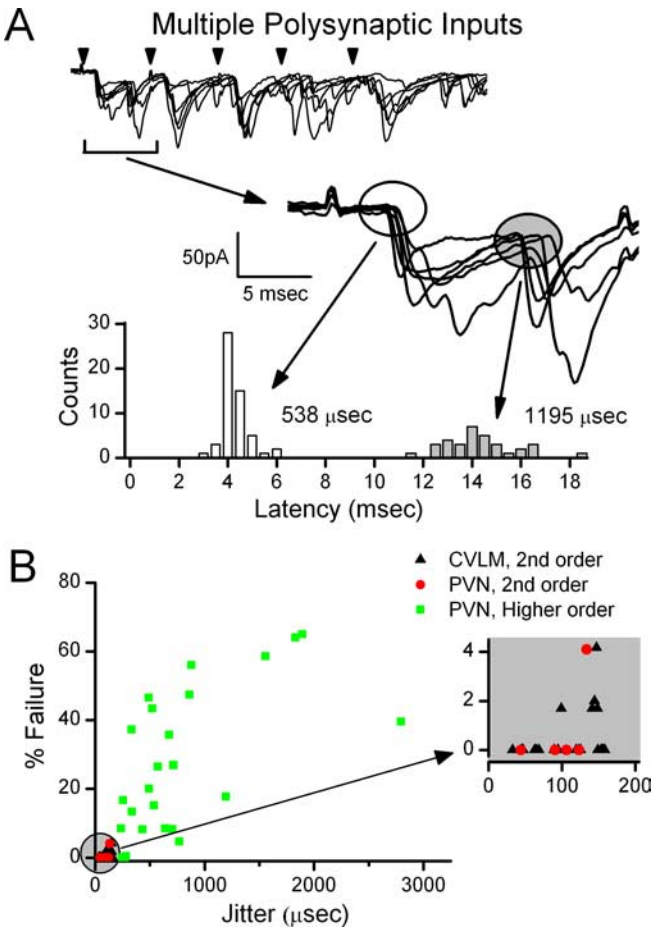

Figure 9. Higher-order, PVN-projecting NTS neurons received variable-latency EPSCs, and often multiple distinct ST inputs indicated convergence on these single neurons. ***A***, In a representative higher-order, PVN-projecting neuron, a single ST shock elicited two, high-jitter synaptic responses that were distinctly separated by latency. As was typical of these polysynaptically coupled neurons, multiple individual EPSCs could be discerned at different latencies in each sweep (***A***, inset). The upper set of current traces shows seven overlaid responses to ST-EPSC bursts (current traces with synaptic failures have been removed for clarity). The inset expands the set of traces to overlay the responses only to the initial ST shock of each burst of five ST shocks (full response displayed above). Ovals mark the regions of analysis for the two unique synaptic inputs to this neuron. The histogram in the bottom portion of ***A*** displays the distributions for the latency values detected for the shorter-latency ST response (open oval) and the longer-latency response (gray oval). Note that this analysis produced two discrete clusters of latency values that reflect the two independent inputs. The jitters for multiple inputs to higher-order PVN neurons were always in the polysynaptic range (>200 μs). ***B***, Summary of failure rates and the relationship to synaptic jitter for all NTS projection neurons. Failure rate is expressed as the percentage of ST shocks failing to evoke a synaptic response. Second-order PVN- and CVLM-projecting NTS neurons expressed very low rates of synaptic failure (inset). Failure rates increased with jitter in higher-order neurons, and thus more complex pathways unreliably transmit afferent signals to higher-order PVN-projecting neurons.

Myelinated and unmyelinated ST pathways activate CVLM- and PVN-projecting neurons

In previous studies, we have shown that ST afferent pathways arising from myelinated and unmyelinated neurons can be distinguished by their susceptibility to blockade by the TRPV (vanilloid receptor) agonist capsaicin (Doyle et al., 2002; Jin et al., 2003). Namely, EPSCs mediated by unmyelinated afferents are typically blocked, whereas EPSCs mediated by myelinated afferents are unaffected. In the present studies, capsaicin (200 nM) blocked ST-evoked EPSCs in two of four CVLM-projecting neurons tested and in two of three second-order PVN-projecting neurons tested (traces not shown). EPSCs in the remaining neurons were unaffected by capsaicin treatment. Capsaicin also blocked ST-evoked polysynaptic EPSCs in three of five cases in higher-order, PVN-projecting neurons. Thus, both myelinated and unmyelinated cranial visceral afferents activate pathways to PVN- and CVLM-projecting neurons.

Discussion

NTS connects extensively and reciprocally with many brain areas that impact the autonomic system, and these links provide broad integration between homeostatic and behavioral networks (Pilowsky and Goodchild, 2002). Neurons in the CVLM and PVN regions receive cranial visceral primary afferent information originating from NTS but serve very different integrative roles (Saper, 2002; Benarroch, 2005). Here, we report substantial systematic differences in the organization and processing of cranial visceral afferent information within NTS that varied by the CNS destination of the NTS neuron output. Using complementary anatomical and electrophysiological techniques, we characterized the intra-NTS links between cranial visceral afferent inputs and two distinct populations of projection neurons: one output to brainstem, CVLM, and the other to forebrain, PVN. Electrophysiological studies found that ST transmission to CVLM-projecting NTS neurons conformed to the performance expectations of simple, direct monosynaptic contacts, and this functional characterization directly mirrored our neuroanatomical results, i.e., second-order neurons. Afferent pathways that reached most PVN-projecting NTS neurons, however, performed with polysynaptic characteristics, a finding that indicates that ST afferent information takes a more convoluted intra-NTS pathway to higher-order, PVN-projecting neurons.

NTS is a highly heterogeneous nucleus (Andresen and Kunze, 1994; Travagli et al., 2006). Multiple histologically defined subregions within the caudal NTS correspond only loosely to specific afferent inputs, neurochemical markers, or efferent destinations (Kalia and Fuxe, 1985; Ruggiero et al., 1994). This fundamental diversity of NTS makes it challenging to tease apart the underlying synaptic and cellular processes that provide the interconnections between neurons within a pathway. Our studies are the first to use both the afferent and efferent context to define specific groups of NTS neurons. This approach has identified differential patterns of pathway connectivity and function, and together shows a physically interleaved network of projection-specific cohorts of NTS neurons that span multiple topographical subregions within NTS.

Cranial afferent intra-NTS pathways: target-specific reliability and convergence patterns

Our studies provide functional performance assays consistent with robust monosynaptic contacts of ST cranial visceral afferents onto CVLM-projecting NTS neurons. ST transmission produced large-amplitude, time-invariant EPSCs that depressed at modest frequencies and rarely failed to generate an EPSC. Changes in stimulus intensity recruited these monosynaptic responses in an all-or-none manner, consistent with activation of single ST axons to each CVLM-projecting neuron (Bailey et al., 2006). Likewise, the low-jitter ST-EPSCs in the present studies closely resemble the synaptic performance of NTS neurons identified anatomically using anterogradely labeled cranial primary afferent terminals (Doyle and Andresen, 2001).

Interestingly, our electron micrographs revealed the presence of multiple axosomatic synaptic contacts that corresponded to confocal images of vagal afferent labeled varicosities on CVLM-projecting neurons. The multiple afferent somatic contacts found

on CVLM-projecting neurons contrasts with our previous work (Aicher et al., 1999) showing that vagal afferent synapses on unidentified NTS cell bodies were extremely rare (one axosomatic compared with 295 axodendritic). However, individual afferent axons can branch extensively within NTS (Donoghue et al., 1981; Davies and Kubin, 1986), and some individual afferents deliver multiple terminal contacts onto the soma and proximal dendrites of single second-order NTS neurons (Anders et al., 1993). Such proximal somatodendritic contacts are consistent with other observations (Miller et al., 1983; Kalia and Richter, 1985; Chan et al., 2000; Sekizawa et al., 2003; Doyle et al., 2004). Synaptic responses recorded in somata isolated from medial NTS suggest that axosomatic terminals share similar afferent pharmacological profiles with those found in more intact preparations (Jin et al., 2004a,b).

Quantal release properties from ST synapses, including baroreceptors, are remarkably homogeneous (Bailey et al., 2006). The synaptic characteristics of ST-EPSCs to CVLM-projecting NTS neurons were remarkably similar and consistent with a high glutamate release probability. This simplest possible intra-NTS pathway structure, ST afferents directly exciting projection neurons, was the only form of transmission elicited by ST shocks that we observed in CVLM-projecting NTS neurons and in a minority of PVN-projecting NTS neurons. High release, proximal ST excitatory synapses may contribute to a high safety factor for transmission to second-order NTS neurons. This presents a fundamentally different model for synaptic integration than the common CNS paradigm of excitatory synaptic inputs arriving on distal dendrites that individually are quite weak and ineffectual (Bruno and Sakmann, 2006).

In contrast to CVLM-projecting neurons, our confocal and electrophysiological analyses suggest that most PVN-projecting neurons do not receive direct input from visceral afferents. The polysynaptic ST pathway to PVN-projecting NTS neurons evoked smaller-amplitude EPSCs that were more variable in timing, with little FDD. Repeated ST shocks intermittently failed to evoke a synaptic response in higher-order PVN-projecting NTS neurons. Thus, ST–NTS–PVN pathways generally include intervening interneurons, i.e., a polysynaptic intra-NTS pathway. Surprisingly, single ST shocks often activated multiple intra-NTS pathways that converged onto single, higher-order PVN-projecting NTS neurons. Receipt of multiple, convergent ST-associated synaptic inputs to higher-order NTS neurons may obscure timing signals from ST afferents and could represent multiple afferent modalities. Interestingly, such convergent, ST-synched inputs were not observed in second-order NTS neurons. A few PVN-projecting NTS neurons displayed monosynaptic ST synaptic responses similar to those in CVLM-projecting neurons. It should be noted that neither anatomical nor electrophysiological studies are likely to detect all synaptic contacts so there is potential for false negatives, undetected physical or functional contacts. The differences in intra-NTS organization suggest systematic differences in local network connections to higher-order neurons. The polysynaptic intra-NTS pathways detected for a majority of PVN-projecting NTS neurons would provide a relatively diffuse afferent signal with inconsistent timing and strength.

Functional implications for afferent pathway performance

CVLM and PVN are key sites associated with autonomic control circuits. The substructure organizing the path to CVLM-projecting neurons was direct and converted afferent action potentials into particularly powerful EPSCs. Synaptic tests of CVLM-projecting neurons revealed innervation likely to arise from a single afferent. Together, the structural organization implied by these synaptic results predicts a remarkably uniform and direct relationship to afferent inputs that should provide a high safety factor (large amplitude) for successfully passing discrete, high-fidelity information to CVLM. Such an intra-NTS pathway organization is quite consistent with reported activity patterns of neurons within CVLM. Activating the aortic depressor nerve, which contains aortic baroreceptors, triggered tightly synchronized spikes in CVLM neurons, and many commonly show synchronization to natural arterial baroreceptor activity (Jeske et al., 1993). The neurons within CVLM are likely GABAergic interneurons that provide rapid inhibition of sympathetic premotor neurons within the rostral ventrolateral medulla during the baroreflex (Aicher et al., 2000; Schreihofer and Guyenet, 2003). Clearly, the fidelity of afferent transmission (close correspondence between afferent spikes and second-order EPSCs) would be significantly degraded by intervening excitatory or inhibitory inputs of different timing. The major synaptic features that we measured in CVLM-projecting NTS neurons support such fidelity, including reliable, large-amplitude ST-EPSCs and an absence of convergent direct afferent or polysynaptic inputs.

The intra-NTS polysynaptic pathway to PVN-projecting NTS neurons performed in a varied and complex manner. In contrast to second-order neurons, higher-order PVN-projecting neurons had multiple, converging ST-synchronized synaptic events, indicating that more than one ST afferent input arrives via separate, polysynaptic intra-NTS paths. Even one ST shock triggered a chaotic barrage of synaptic inputs that arrived scattered across time and, when repeated, failed on different trials. An important aspect of the safety factor for afferent information going forward was relatively low (small-amplitude EPSCs), and thus successful transmission to PVN was less likely. In addition, if more than one afferent converges onto these neurons, then these polysynaptically coupled, PVN-projecting neurons will convey mixed afferent information and provide sensory integration at the level of NTS. In most PVN neurons *in vivo*, activation of arterial baroreceptors evokes temporally diffuse, weak cardiovascular afferent signals (Kannan and Yamashita, 1983), responses that were quite consistent with the intra-NTS transmission properties observed in most PVN-projecting NTS neurons. In contrast, a subpopulation of spinally projecting PVN neurons are both synchronized to cardiovascular rhythms and highly responsive to baroreflex activation (Chen and Toney, 2003). Such characteristics raise the possibility that this small population of neurons may be activated by second-order PVN-projecting NTS neurons. Although we focused discussions of PVN and CVLM function primarily in relation to cardiovascular system targets, both of these regions contribute substantially to many other homeostatic systems, and these pathways consist of similarly heterogeneous neurons that anatomically overlap and intermix with cardiovascular circuits (Kubin et al., 2006). Despite this functional diversity, afferent processing patterns were quite uniform for the NTS–CVLM pathway compared with signals directed to PVN.

We delineated key functional distinctions that arise from the local organization of intra-NTS pathways. These pathway characteristics impact the quality and strength of cranial visceral afferent information reaching NTS output neurons. The translation of synaptic inputs into action potentials, however, will depend on postsynaptic neuron characteristics. Thus, excitatory synaptic current amplitude is one aspect of safety factor for faithful transmission (propagating action potentials), but reliable output will also depend on postsynaptic properties such as potassium channel expression that differs substantially across NTS

neurons (Bailey et al., 2002). Such postsynaptic characteristics of the NTS projection neurons may further transform and tune the character of the cranial visceral afferent information transmitted to distant targets.

References

Aicher SA, Kurucz OS, Reis DJ, Milner TA (1995) Nucleus tractus solitarius efferent terminals synapse on neurons in the caudal ventrolateral medulla that project to the rostral ventrolateral medulla. Brain Res 693:51–63.

Aicher SA, Saravay RH, Cravo S, Jeske I, Morrison SF, Reis DJ, Milner TA (1996) Monosynaptic projections from the nucleus tractus solitarii to C1 adrenergic neurons in the rostral ventrolateral medulla: comparison with input from the caudal ventrolateral medulla. J Comp Neurol 373:62–75.

Aicher SA, Sharma S, Cheng PY, Pickel VM (1997) The *N*-methyl-D-aspartate (NMDA) receptor is postsynaptic to substance P-containing axon terminals in the rat superficial dorsal horn. Brain Res 772:71–81.

Aicher SA, Sharma S, Pickel VM (1999) *N*-methyl-D-aspartate receptors are present in vagal afferents and their dendritic targets in the nucleus tractus solitarius. Neuroscience 91:119–132.

Aicher SA, Milner TA, Pickel VM, Reis DJ (2000) Anatomical substrates for baroreflex sympathoinhibition in the rat. Brain Res Bull 51:107–110.

Anders K, Ohndorf W, Dermietzel R, Richter DW (1993) Synapses between slowly adapting lung stretch receptor afferents and inspiratory beta-neurons in the nucleus of the solitary tract of cats: a light and electron microscopic analysis. J Comp Neurol 335:163–172.

Andresen MC, Kunze DL (1994) Nucleus tractus solitarius: gateway to neural circulatory control. Annu Rev Physiol 56:93–116.

Bailey TW, Jin YH, Doyle MW, Andresen MC (2002) Vanilloid-sensitive afferents activate neurons with prominent A-type potassium currents in nucleus tractus solitarius. J Neurosci 22:8230–8237.

Bailey TW, Nicol GD, Schild JH, DiMicco JA (2003) Synaptic and membrane properties of neurons in the dorsomedial hypothalamus. Brain Res 985:150–162.

Bailey TW, Jin YH, Doyle MW, Smith SM, Andresen MC (2006) Vasopressin inhibits glutamate release via two distinct modes in the brainstem. J Neurosci 26:6131–6142.

Benarroch EE (2005) Paraventricular nucleus, stress response, and cardiovascular disease. Clin Auton Res 15:254–263.

Bruno RM, Sakmann B (2006) Cortex is driven by weak but synchronously active thalamocortical synapses. Science 312:1622–1627.

Chan RK, Peto CA, Sawchenko PE (2000) Fine structure and plasticity of barosensitive neurons in the nucleus of solitary tract. J Comp Neurol 422:338–351.

Chen QH, Toney GM (2003) Identification and characterization of two functionally distinct groups of spinal cord-projecting paraventricular nucleus neurons with sympathetic-related activity. Neuroscience 118:797–807.

Ciriello J (1983) Brainstem projections of aortic baroreceptor afferent fibers in the rat. Neurosci Lett 36:37–42.

Dampney RAL, Horiuchi J, Killinger S, Sheriff M, Tan P, McDowall L (2005) Long-term regulation of arterial blood pressure by hypothalamic nuclei: some critical questions. Clin Exp Pharmacol Physiol 32:419–425.

Davies RO, Kubin L (1986) Projection of pulmonary rapidly adapting receptors to the medulla of the cat: an antidromic mapping study. J Physiol (Lond) 373:63–86.

Donoghue S, Fox RE, Kidd C, Koley BN (1981) The distribution in the cat brain stem of neurones activated by vagal non-myelinated fibres from the heart and lungs. Q J Exp Physiol 66:391–404.

Doyle MW, Andresen MC (2001) Reliability of monosynaptic transmission in brain stem neurons in vitro. J Neurophysiol 85:2213–2223.

Doyle MW, Bailey TW, Jin YH, Andresen MC (2002) Vanilloid receptors presynaptically modulate visceral afferent synaptic transmission in nucleus tractus solitarius. J Neurosci 22:8222–8229.

Doyle MW, Bailey TW, Jin YH, Appleyard SM, Low MJ, Andresen MC (2004) Strategies for cellular identification in nucleus tractus solitarius slices. J Neurosci Methods 37:37–48.

Duan YF, Kopin IJ, Goldstein DS (1999) Stimulation of the paraventricular nucleus modulates firing of neurons in the nucleus of the solitary tract. Am J Physiol 277:R403–R411.

Guyenet PG (2006) The sympathetic control of blood pressure. Nat Rev Neurosci 7:335–346.

Herman JP, Figueiredo H, Mueller NK, Ulrich-Lai Y, Ostrander MM, Choi DC, Cullinan WE (2003) Central mechanisms of stress integration: hierarchical circuitry controlling hypothalamo-pituitary-adrenocortical responsiveness. Front Neuroendocrinol 24:151–180.

Hermes SM, Mitchell JL, Aicher SA (2006) Most neurons in the nucleus tractus solitarii do not send collateral projections to multiple autonomic targets in the rat brain. Exp Neurol 198:539–551.

Jeske I, Morrison SF, Cravo SL, Reis DJ (1993) Identification of baroreceptor reflex interneurons in the caudal ventrolateral medulla. Am J Physiol 264:R169–R178.

Jin YH, Bailey TW, Doyle MW, Li BY, Chang KSK, Schild JH, Mendelowitz D, Andresen MC (2003) Ketamine differentially blocks sensory afferent synaptic transmission in medial nucleus tractus solitarius (mNTS). Anesthesiology 98:121–132.

Jin YH, Bailey TW, Li BY, Schild JH, Andresen MC (2004a) Purinergic and vanilloid receptor activation releases glutamate from separate cranial afferent terminals. J Neurosci 24:4709–4717.

Jin YH, Bailey TW, Andresen MC (2004b) Cranial afferent glutamate heterosynaptically modulates GABA release onto second order neurons via distinctly segregated mGluRs. J Neurosci 24:9332–9340.

Kalia M, Fuxe K (1985) Rat medulla oblongata. I. Cytoarchitectonic considerations. J Comp Neurol 233:285–307.

Kalia M, Richter D (1985) Morphology of physiologically identified slowly adapting lung stretch receptor afferents stained with intra-axonal horseradish peroxidase in the nucleus of the tractus solitarius of the cat. II. An ultrastructural analysis. J Comp Neurol 241:521–535.

Kannan H, Yamashita H (1983) Electrophysiological study of paraventricular nucleus neurons projecting to the dorsomedial medulla and their response to baroreceptor stimulation in rats. Brain Res 279:31–40.

Kubin L, Alheid GF, Zuperku EJ, McCrimmon DR (2006) Central pathways of pulmonary and lower airway vagal afferents. J Appl Physiol 101:618–627.

Maley BE (1996) Immunohistochemical localization of neuropeptides and neurotransmitters in the nucleus solitarius. Chem Senses 21:367–376.

Mendelowitz D, Yang M, Andresen MC, Kunze DL (1992) Localization and retention in vitro of fluorescently labeled aortic baroreceptor terminals on neurons from the nucleus tractus solitarius. Brain Res 581:339–343.

Miller AJ, McKoon M, Pinneau M, Silverstein R (1983) Postnatal synaptic development of the nucleus tractus solitarius (NTS) of the rat. Dev Brain Res 8:205–213.

Pilowsky PM, Goodchild AK (2002) Baroreceptor reflex pathways and neurotransmitters: 10 years on. J Hypertens 20:1675–1688.

Ruggiero DA, Pickel VM, Milner TA, Anwar M, Otake K, Mtui EP, Park D (1994) Viscerosensory processing in nucleus tractus solitarii: structural and neurochemical substrates. In: Nucleus of the solitary tract (Barraco RA, ed), pp 3–34. Boca Raton, FL: CRC.

Saper CB (2002) The central autonomic nervous system: conscious visceral perception and autonomic pattern generation. Annu Rev Neurosci 25:433–469.

Schreihofer AM, Guyenet PG (2003) Baro-activated neurons with pulse-modulated activity in the rat caudal ventrolateral medulla express GAD67 mRNA. J Neurophysiol 89:1265–1277.

Sekizawa S, Joad JP, Bonham AC (2003) Substance P presynaptically depresses the transmission of sensory input to bronchopulmonary neurons in the guinea pig nucleus tractus solitarii. J Physiol (Lond) 552:547–559.

Spyer KM (1990) The central nervous organization of reflex circulatory control. In: Central regulation of autonomic functions (Loewy AD, Spyer KM, eds), pp 168–188. New York: Oxford UP.

Stern JE (2001) Electrophysiological and morphological properties of pre-autonomic neurones in the rat hypothalamic paraventricular nucleus. J Physiol (Lond) 537:161–177.

Travagli RA, Hermann GE, Browning KN, Rogers RC (2006) Brainstem circuits regulating gastric function. Annu Rev Physiol 68:279–305.

Trussell LO (1999) Synaptic mechanisms for coding timing in auditory neurons. Annu Rev Physiol 61:477–496.

Weston M, Wang H, Stornetta RL, Sevigny CP, Guyenet PG (2003) Fos expression by glutamatergic neurons of the solitary tract nucleus after phenylephrine-induced hypertension in rats. J Comp Neurol 460:525–541.

Zucker RS, Regehr WG (2002) Short-term synaptic plasticity. Annu Rev Physiol 64:355–405.